Observer Design for an Experimental Rotor System with Discontinuous Friction

A. Lj. Juloski, N. Mihajlović, W. P. M. H. Heemels, N. van de Wouw and H. Nijmeijer

Abstract— **In this paper we present an experimental observer design for a rotor system with friction. The model of the system exhibits set-valued static friction law with the Stribeck effect. As the model of the setup is non-smooth and non-Lipschitz, observer has to be designed using mathematical tools from convex analysis and the theory of differential inclusions. The designed observer guarantees that there exists a unique solution to the observer dynamics and that the estimated state converges to the true state of the system. Simulation and experimental results illustrate the design and performance of the observer in practice.**

I. INTRODUCTION

In this paper we present an experimental observer design for a rotor system with friction. The experimental setup was introduced in [1], [2]. There, the focus was on analysis of the nonlinear dynamics of the setup, and in particular on friction-induced limit cycling.

The experimental set-up consists of two discs, connected through a low-stiffness string. The upper disc is driven by a motor and a brake applied to the lower disc exerts a friction force on the disc. The friction at the lower disc can be accurately described by a nonlinear set-valued friction law with negative damping in a certain range of angular velocities (Stribeck effect) [1].

The rotor system with friction has been designed in order to study friction-induced limit cycling that is present in a wide variety of mechanical systems with friction and flexibilities. It should be noted that the configuration of the experimental setup (two masses, coupled by a flexible element, of which one is subject to friction and the other is driven by an actuator) can be recognized in many other mechanical systems, in which friction deteriorates the system performance by the introduction of vibrations. In this context, one can think of drilling rigs [3]–[5], printers, turbine blade dampers [6], industrial and domestic robots [7], simple earth-quake models, curve squealing of railway vehicles [8], accurate mirror positioning systems on satellites and many more. In many mechanical systems, friction-induced limit cycling often limits the performance and endangers the safety of operation, and hence, should be controlled and suppressed. As it is usually hard to measure the complete system state, observers form a necessary part if a state feedback control law has to be implemented.

Due to the presence of a set-valued friction force, the system dynamics is non-smooth and non-Lipschitz. We propose a Luenberger type observer, which contains a copy of the system dynamics, and output error injection terms. Since the proposed observer is non-smooth, tools of non-smooth analysis are used to formally analyze and prove its properties. Moreover, because the considered systems is non-Lipschitz, the existence and uniqueness of solutions (i.e. well-posedness) of the observer dynamics is not a priori guaranteed. Well-posedness of the observer is necessary to ensure proper behavior of the numerical implementation. The proposed observer design methodology guarantees that the solution of the proposed observer exists, and that the estimated state converges to the true state of the system. The design of the proposed observer is based on [9], [10].

The paper is structured as follows. In section II, some elementary notions from convex analysis and the theory of differential inclusions are given. In section III, we present the observer design, together with the theoretical results that establish the correctness of the proposed design procedure. The experimental rotor system with friction is described in section IV, together with the model and the parameter identification procedure. Simulation and experimental results are presented in sections V and VI. Finally, in section VII concluding remarks are given.

II. PRELIMINARIES

The material in this section is taken from [11], [12], [13].

With $\mathcal{L}^1_{loc}[0,\infty)$ and $\mathcal{L}^2_{loc}[0,\infty)$ we denote the Lebesgue spaces of locally integrable and square integrable functions defined on $[0,\infty)$.

A mapping $\rho : \mathbb{X} \to \mathbb{Y}$, where $\mathbb{X}, \mathbb{Y} \subseteq \mathbb{R}^l$, is said to be *multivalued* if it assigns to each element $x \in \mathbb{X}$ a subset $\rho(x) \subset \mathbb{Y}$ (which may be empty). The domain of the mapping $\rho(\cdot)$, $\operatorname{dom}\rho$ is defined as $\operatorname{dom}\rho = \{x | x \in \mathbb{X}, \rho(x) \neq \emptyset\}$. We define the graph of the mapping ρ as:

$$\operatorname{Graph}\rho = \{(x, x^*) \mid x^* \in \rho(x)\}. \tag{1}$$

A multivalued mapping ρ is said to be *monotone* if

$$\forall x_1, x_2 \in \operatorname{dom}\rho, \quad \forall x_1^* \in \rho(x_1) \forall x_2^* \in \rho(x_2)$$
$$\langle x_1^* - x_2^*, x_1 - x_2 \rangle \geq 0,$$

where $\langle \cdot, \cdot \rangle$ denotes the inner product in $\mathbb{R}^l$.

This work is partially supported by European project grants SICONOS (IST2001-37172) and HYCON Network of Excellence, contract number FP6-IST-511368

Aleksandar Juloski is with with the Department of Electrical Engineering, Eindhoven University of Technology, P.O. Box 513, 5600 MB Eindhoven, The Netherlands, E-mail: a.juloski@tue.nl.

Nenad Mihajlović is with Philips Research, Eindhoven, The Netherlands, E-mail:nenad.mihajlovic@philips.com

Maurice Heemels is with the Embedded Systems Institute, P.O. Box 513, 5600 MB Eindhoven, The Netherlands, E-mail: maurice.heemels@embeddedsystems.nl.

Nathan van de Wouw and Henk Nijmeijer are with the Department of Mechanical Engineering, Eindhoven University of Technology, P.O. Box 513, 5600 MB Eindhoven, The Netherlands, E-mail: {n.v.d.wouw, h.nijmeijer}@tue.nl

A multivalued mapping ρ is said to be *maximally monotone* if its graph is not strictly contained in the graph of any other monotone mapping. In other words, maximality means that new elements can not be added to $\mathrm{Graph}\,\rho$ without violating the monotonicity of the mapping. Examples of maximal monotone mappings can be found in many mechanical and electrical systems. In figure 1a, the force characteristic of a one-sided spring is given. Note that this mapping is single valued and maximal monotone. In figure 1b, an ideal dry friction characteristic is depicted. Figure 1c depicts the characteristic of the ideal diode or an unilateral contact law in mechanics, while 1d depicts the characteristic of the MOSFET transistor.

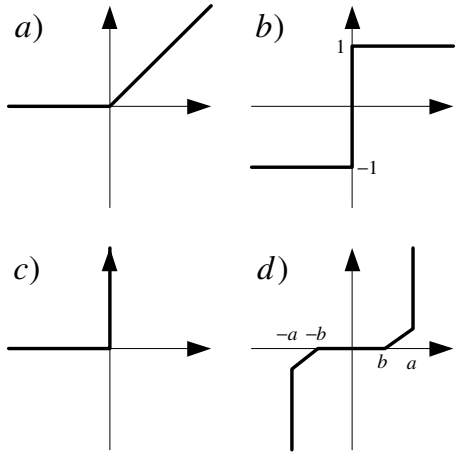

Fig. 1. Examples of maximal monotone mappings

A *differential inclusion* (DI) is given by an expression of the form

$$\dot{x}(t) \in F(t, x(t)), \tag{2}$$

where F is a set-valued mapping, that associates to the state x of the system and time t the set of admissible velocities. An *absolutely continuous* (AC) function x is considered to be a *strong solution* of the DI (2) if (2) is satisfied almost everywhere. Following [12, section 3.2] we define a continuous function x to be a *weak solution* to (2) if there exist a sequence $x_n \in \mathcal{C}[0,\infty)$ such that x_n is a strong solution to

$$\dot{x}_n \in F(t, x_n(t)),$$

and $x_n \to x$ uniformly on $[0,\infty)$. A point x_0 is a *fixed point (equilibrium)* of the DI (2) if

$$0 \in F(t, x_0),\ \forall t.$$

Following [14, theorem 1], we call a linear system given by the triple (A, B, C), where B has full column rank (i.e. $\mathrm{Ker}\{B\} = \{0\}$), strictly positive real (SPR) if there exist a $P = P^\top > 0$ and a $Q = Q^\top > 0$ such that:

$$PA + A^\top P = -Q \tag{3a}$$
$$B^\top P = C \tag{3b}$$

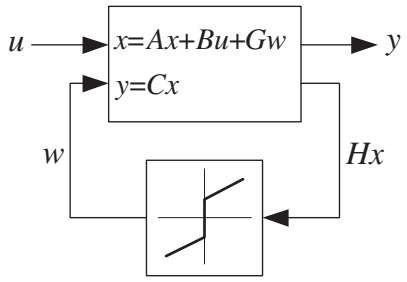

Fig. 2. System with maximal monotone multivalued mapping in the feedback path.

III. OBSERVER DESIGN

Consider the system given by the following differential inclusion (see figure 2):

$$\dot{x} \in Ax - G\varrho(Hx) + Bu \tag{4a}$$
$$y = Cx, \tag{4b}$$

where $Hx(0) \in \mathrm{dom}\,\varrho$ and $A \in \mathbb{R}^{n\times n}$, $B \in \mathbb{R}^{n\times m}$. $G \in \mathbb{R}^{n\times l}$ is full column rank, $H \in \mathbb{R}^{l\times n}$ and $C \in \mathbb{R}^{p\times n}$. The mapping $\varrho : \mathbb{R}^l \to \mathbb{R}^l$ is assumed to be maximally monotone.

Assumption III.1 For all initial states $x(0)$ such that $Hx(0) \in \mathrm{dom}\,\varrho$ and inputs $u \in \mathcal{L}^1_{loc}[0,\infty)$ of interest, we assume that the system (4) has a strong solution.

The proposed observer is a differential inclusion of the following form:

$$\dot{\hat{x}} \in (A - LC)\hat{x} - G\varrho((H - KC)\hat{x} + Ky) + Ly + Bu \tag{5a}$$
$$\hat{y} = C\hat{x}, \tag{5b}$$

where $K \in \mathbb{R}^{l\times p}$ and $\hat{x}(0)$ are such that $(H - KC)\hat{x}(0) + Ky(0) \in \mathrm{dom}\,\varrho(\cdot)$.

The problem of observer design consists of finding the gains L, K which will guarantee that there exists a (unique) solution $\hat{x}$ to the observer dynamics on $[0,\infty)$. Moreover, it is required that $\hat{x}(t) \to x(t)$ as $t \to \infty$.

Remark III.2 If the mapping ϱ is single valued, differential inclusions (4) and (5) become differential equations. If the mapping ρ also satisfies certain additional conditions (e.g. the mapping is locally Lipschitz), Lipschitz conditions that guarantee existence and uniqueness of solutions apply to both (4) and (5). An observer design methodology for systems of type (4) with *single valued*, *locally Lipschitz* and *slope restricted* nonlinearities in the feedback path was presented in [15]. Since set-valued and non-Lipschitz nonlinearities are allowed in the class of systems studied here, the results of [15] are not applicable. Instead we have to resort to a framework of convex analysis, to establish an observer design procedure for the considered class of systems.

In this section we will show that if L and K are chosen such that the triple $(A-LC, G, H-KC)$ is SPR the obtained observer (5) will satisfy the mentioned requirements.

Before we prove this we will first show how the gains L and K can be computed such that $(A-LC, G, H-KC)$ is SPR. This can be achieved by solving the matrix inequality:

$$\begin{aligned}(A-LC)^\top P + P(A-LC) &< 0 \quad (6a)\\ G^\top P &= H - KC. \quad (6b)\end{aligned}$$

Inequality (6) is a linear matrix inequality in P,K,$L^\top P$. For necessary and sufficient conditions for the existence of solutions for (6), see for instance, [15].

Theorem III.3 *Consider the system* (4)*, under assumption III.1, and the observer* (5)*. If the triple* $(A-LC, G, H-KC)$ *is SPR, then there exists a unique weak solution to the observer dynamics* (5) *on* $[0,\infty)$.

For the proof of theorem III.3, see [9].

For the observer (5) the observation error $e := x - \hat{x}$ dynamics can be formed as:

$$\dot{e} = (A-LC)e - G(w-\hat{w}) \quad (7a)$$
$$w \in \varrho(Hx) \quad (7b)$$
$$\hat{w} \in \varrho(H\hat{x} + K(y-\hat{y})). \quad (7c)$$

The following theorem proves the asymptotic stability of the designed observer.

Theorem III.4 *Consider the observed system* (4) *under assumption III.1, the observer* (5)*, where the triple* $(A-LC, G, H-KC)$ *is SPR, and the observation error dynamics* (7)*. Then, the point* $e=0$ *is the unique fixed point of the observation error dynamics* (7) *and is globally exponentially stable. Moreover, the following bound holds:*

$$\frac{1}{2}\lambda_{min}(P)e^\top(t)e(t) \le e^\top(0)Pe(0)\exp\left(-\frac{\lambda_{min}(Q)}{\lambda_{min}(P)}t\right). \quad (8)$$

where $\lambda_{min}(\cdot)$ *denotes the minimal eigenvalue, and the matrices* P *and* Q *are given by* (3)*.*

For the proof of theorem III.4, see [9].

Remark III.5 Note that the uniqueness of the solutions of the original system (4) is not required for the well-posedness of the observer (5). Indeed, theorems III.3 and III.4 state that when supplied with the input and output signals of the original system u and y, respectively, the solution of the observer dynamics (5) exists and is unique, and that the estimated state $\hat{x}$ will converge to the actual state of the observed system x for $t \to \infty$.

Solutions $\hat{x}(\cdot)$ of the observer (5) can be obtained using numerical methods for solving differential inclusions. See e.g. the survey article [16]. To give briefly one numerical method, we aim to approximate the solution $\hat{x}(\cdot)$ of the DI (5) with a piecewise constant function $\eta(\cdot)$, where $\eta(t)=\eta(t_k)$ for $t \in [t_k, t_{k+1})$, $t_{k+1}-t_k = h$, for a given step size h. In particular, for the class of DIs of the form

$$\dot{\hat{x}} \in -A(t,x), \quad (9)$$

where $A(\cdot,\cdot)$ is a maximal monotone mapping, the approximations of the (unique) solution with good numerical properties (e.g. no chattering) can be computed using implicit Runge-Kutta methods [17]. For instance, the *implicit midpoint rule* takes the following form:

$$\eta(t_{k+1}) \in \eta(t_k) - hA(t_k + \frac{1}{2}h, \frac{1}{2}(\eta(t_k)+\eta(t_{k+1}))), \quad (10)$$

which has first-order of convergence as a function of h, on time intervals where the solution $\hat{x}$ is twice continuously differentiable. See [16], [17] for more details and numerical methods with a higher order of convergence.

IV. EXPERIMENTAL ROTOR SYSTEM WITH FRICTION

The experimental rotor system with friction is shown in figure 3. The input voltage from the computer, which is between $-5\,\mathrm{V}$ and $5\,\mathrm{V}$, is fed into the DC-motor via the power amplifier. The DC-motor is connected to the upper steel disc, via a gear box. The upper and lower disc are connected through a low stiffness steel string. Both discs can rotate around their respective geometric centers and the related angular positions are measured using incremental encoders. The angular velocities of both discs can be obtained by numerical differentiation of the angular positions and filtering the resulting signals using a low-pass filter. Moreover, an additional brake is applied at the lower brass disc. The contact material of the brake is rubber.

The rotor system with friction is a mechanical system and it can be described by the following first-principle model:

$$\begin{aligned}J_u\ddot{\theta}_u + k_\theta(\theta_u-\theta_l) + T_{fu}(\dot{\theta}_u) &= k_m\,u\\ J_l\ddot{\theta}_l - k_\theta(\theta_u-\theta_l) + T_{fl}(\dot{\theta}_l) &= 0,\end{aligned} \quad (11)$$

where θ_u and θ_l are the angular positions of the upper and lower discs, respectively. The voltage u is the input voltage to the power amplifier of the motor, J_u and J_l are moments of inertia of the upper and lower discs about their respective centers of mass, k_θ is the torsional spring stiffness and k_m is the motor constant. T_{fu} and T_{fl} denote friction torques acting on the upper and lower discs, respectively. It should be noted that the friction torque at the upper disc $T_{fu}(\dot{\theta}_u)$ is due to friction in the bearings of the upper disc and due to the electro-magnetic effects in the DC-motor. The friction torque at the lower disc $T_{fl}(\dot{\theta}_l)$ comprises the friction in the bearings of the lower disc and the friction induced by the brake-mechanism (for more details see [1]).

The dynamics of the fourth-order system (11), can be described by a third-order state-space system since its dynamics is independent of the angular positions of the discs but only depends on the difference between these two angular positions. Therefore, by choosing state variables as $x_1 = \theta_u - \theta_l$, $x_2 = \dot{\theta}_u$ and $x_3 = \dot{\theta}_l$, the following state-space model can be obtained

$$\dot{x}_1 = x_2 - x_3 \quad (12a)$$
$$\dot{x}_2 = \frac{k_m}{J_u}u - \frac{k_\theta}{J_u}x_1 - \frac{1}{J_u}T_{fu}(x_2) \quad (12b)$$
$$\dot{x}_3 = \frac{k_\theta}{J_l}x_1 - \frac{1}{J_l}T_{fl}(x_3). \quad (12c)$$

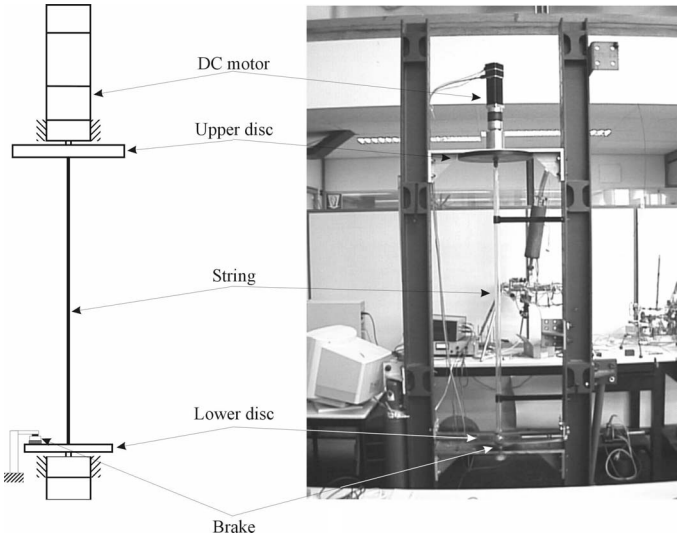

Fig. 3. Experimental rotor system with friction.

In order to complete the model of the system, we need to estimate the parameters k_m, J_u, J_l, k_θ and the nonlinear maps $T_{fu}(\dot{\theta}_u)$ and $T_{fl}(\dot{\theta}_l)$. The experimental identification procedure is briefly described below. For more detailed information on the identification procedure and validation results we refer to [1], [2].

First, the upper disc is disconnected from the lower disc and the parameters concerning the motor and the upper disc (k_m, J_u and $T_{fu}(\dot{\theta}_u)$) are estimated. The estimation process is based on dedicated experiments involving responses of the system, when constant and white noise input voltages u are applied, and an identification procedure (based on nonlinear least-squares approach) ensuring a close match between the model predictions and experimental results. The estimated procedure indicates that at the upper disc $T_{fu}(x_2)$ the viscous friction due to the electro-magnetic effect in the motor dominates, and for simplicity reasons we take that $T_{fu}(x_2) = b_{up}x_2$.

In order to estimate the remaining parameters of the setup (k_θ, J_l) and the friction torque at the lower disc ($T_{frl}(x_3)$), the upper and lower disc are connected again via the low stiffness string and a quasi-random voltage signal is applied to the motor. During the parameter estimation of the model, it is observed that the friction at the lower disc can accurately be modelled with a set-valued humped friction model [1]. Hereto, the following set-valued torque law for the friction is used:

$$T_{fl}(x_3) = \begin{cases} (T_{sl} + T_1(1 - \frac{2}{1+e^{w_1|x_3|}}) + \\ \qquad T_2(1 - \frac{2}{1+e^{w_2|x_3|}}))\,\mathrm{sign}(x_3) + b_l x_3 \\ \qquad\qquad \text{for } x_3 \neq 0 \\ [-T_{sl}, T_{sl}] \\ \qquad\qquad \text{for } x_3 = 0 \end{cases} \tag{13}$$

where T_{sl}, T_1, T_2, w_1, w_2 and b_l are the parameters of the friction model. Moreover, $-T_{sl}$ and T_{sl} represent the minimum and the maximum static friction level, respectively, and b_l is the viscous friction coefficient.

The parameters of the friction model (13) are estimated using a nonlinear least-squares technique. Hereto, persistently exciting input voltage signals are taken as inputs for the experimental system and the angular positions of both discs are measured. Next, the response of the model to such inputs is simulated and an optimal set of parameter estimates is calculated based on matching the measurements and simulations in a least-squares sense. The identified parameters of the model (12) are given in table I. The friction law (13) with the parameters from table I is depicted in the figure (4).

TABLE I

PARAMETER VALUES OF THE MODEL (12), (13).

Parameter		Estimated value
J_u	[kg m^2/rad]	0.4765
k_m	[Nm/V]	3.9950
b_{up}	[Nms/rad]	2.2247
k_θ	[Nm/rad]	0.0727
J_l	[kg m^2/rad]	0.0326
T_{sl}	[Nm]	0.1642
T_1	[Nm]	0.0603
T_2	[Nm]	-0.2267
w_1	[s/rad]	5.7468
w_2	[s/rad]	0.2941
b_l	[Nms/rad]	0.0109

The mapping which describes the friction force at the lower disc is not monotone, see figure 4, but can be transformed into a monotone mapping using the technique of loop transformation [18]. The new friction mapping is defined as $\tilde{T}_{fl}(\omega) = T_{fl}(\omega) - m\omega$, where $m = -0.02$ is the maximal negative slope of the graph in figure 4. The system matrix A is replaced by $\tilde{A} = A - mGH$. The model of the setup now takes the form:

$$\dot{x} \in \tilde{A}x + Bu - G\tilde{T}_{fl}(Hx) \tag{14}$$

which is in the form (4). The values of B, G and H matrices can be easily inferred from (12).

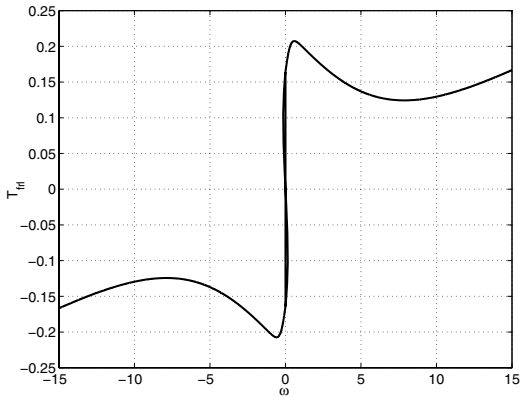

Fig. 4. Dry friction characteristic at the lower disc

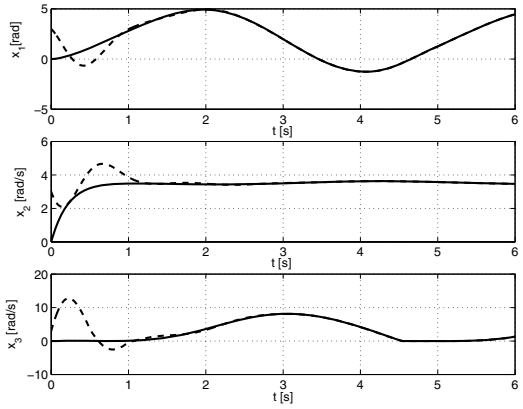

Fig. 5. Simulated responses of the system (solid) and the observer (dashed): x_1 (upper), x_2 (in the middle), x_3 (lower) under the constant input voltage

It should be noted that although the friction model is relatively simple (static), it allows to accurately describe the discontinuous dynamics of the system (see [2]). Now, the observer design proposed in section III allows to deal with such discontinuities and effectively use the model for state-estimation purposes.

V. OBSERVER DESIGN AND SIMULATION RESULTS

Both angular displacements in the experimental setup can be measured. For the observer design, we will use

$$y = x_1$$

(i.e. the difference between the angular positions of the two discs) as a measured output, while the observer will provide both estimates for the other two state variables (velocities of both discs). We will compare the estimated values of the states x_2 and x_3 with the measured values, as a way to validate the designed observer.

The design of the observer of the form (5) for system (14) entails finding gains L and K such that the triple $(\tilde{A} - LC, G, H - KC)$ is SPR. Using LMITOOL for MATLAB (6) the following values for P, Q,L and K were found:

$$P = \begin{bmatrix} 0.804 & 0.029 & 0.066 \\ 0.029 & 0.110 & -0.000 \\ 0.066 & -0.000 & 0.032 \end{bmatrix},$$

$$Q = \begin{bmatrix} 0.548 & -0.000 & -0.000 \\ -0.000 & 0.970 & -0.036 \\ -0.000 & -0.036 & 0.092 \end{bmatrix},$$

$$L = \begin{bmatrix} 2.476 & 5.199 & -26.220 \end{bmatrix}^\top, \; K = -2.025.$$

In this section we will show simulations, and in the next section we will show experimental results. Simulations will allow us to demonstrate the performance of the designed observer under ideal conditions, i.e. the input-output data supplied to the observer is generated by the model which was used for the observer design. Although the identified model of the setup is relatively accurate [1], [2], a number of effects not in the model (such as: parasitic dynamics, sensor errors, delays in data acquisition and processing) may influence the experimental performance of the observer.

The input signal u in (12) is chosen to be a constant signal, $u = 2$V. When a constant input voltage is applied (i.e. a constant torque is applied to the upper disc) slip-stick oscillations (torsional vibrations) occur due to the negative damping in the friction law (13). During these oscillations the velocity of the third disc alternates between 0 (stick phase), and a positive value (slip phase). It is easy to check that for the chosen input signal the system (12) satisfies the conditions of [19, theorem 2.7.1], and hence has a solution on a arbitrarily long time interval for every initial condition x_0, i.e. the system (12) satisfies assumption III.1.

We will show simulations for the initial state for the system taken as $x(0) = [0 \quad 0 \quad 0]^\top$ and for the observer as $\hat{x}(0) = [3 \quad 3 \quad 3]^\top$. The solution of the system (12) is constructed using the dedicated technique for simulating systems with discontinuous friction models presented in [20]. Observer is simulated using (10).

The simulation results are depicted in figure 5 and the estimation error is depicted in figure 6. As guaranteed by the theory, the designed observer is able to provide a correct estimate of the state. Moreover, based on (8) we can provide a bound on the decrease of the squared estimation error. This is indicated by the dashed line in figure 6.

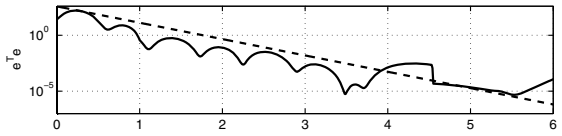

Fig. 6. The norm of the simulated estimation error (solid) and the theoretical bound of the error norm (8) (dashed), in logarithmic scale.

From figures 5 and 6 we see that the estimation error of the observer does not converge to zero, but oscillates around a small residual value ($\approx 10^{-3}$). This residual error can be accounted for by recalling the numerical schemes that are used to simulate the system and the observer provide only

approximations of the true solution.

VI. EXPERIMENTAL RESULTS

The responses of the experimental setup are measured under the same conditions as for simulations (i.e. the input voltage $u = 2\text{V}$), and the designed observer is applied for the state estimation. Measured and estimated states are depicted in figure 7. The experimental estimation error is depicted in figure 8, together with the theoretical bound (8).

The experimental results show that the designed observer is able to provide accurate estimates of the states. The estimation error does not converge to zero, but oscillates around the value of $\approx 10^{-1}$. This error is small compared to the magnitude of the states, but larger than in the simulations. Some causes that may contribute to this residual error are model and sensor errors.

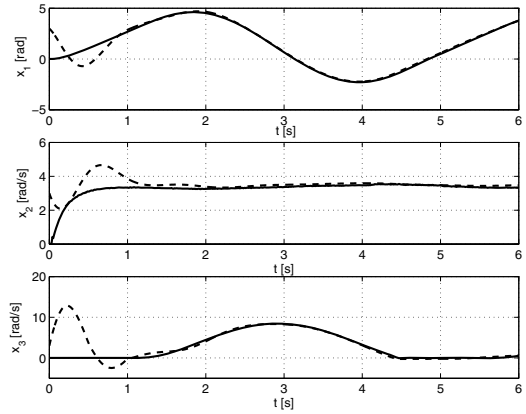

Fig. 7. Measured responses (solid) and the estimation (dashed): x_1 (upper), x_2 (in the middle), x_3 (lower) under the constant input voltage $u = 2\text{V}$.

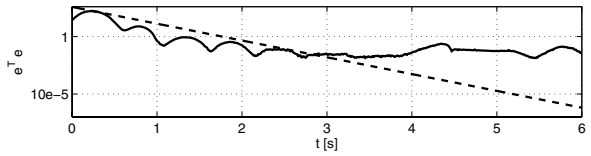

Fig. 8. The norm of the experimental estimation error(solid) and the theoretical bound of the error norm (8) (dashed), on a logarithmic scale

VII. CONCLUSIONS

In this paper we have presented an observer design for an experimental rotor system with friction. The model of the experimental setup was obtained starting from first principles and the unknown model parameters were experimentally identified. Simple static set-valued friction law was used to model the friction.

Since the model of the setup is non-smooth and non-Lispchitz, observer design techniques for smooth nonlinear systems do not apply. To design the observer we used the framework of convex analysis and differential inclusions. The model-based observer allows to effectively exploit the predictive qualities of the discontinuous model of the dynamics.

The performance of the designed observer was demonstrated by both simulation and experimental results. In both simulations, when the model of the system perfectly matches the model within the observer, and experiments, the designed observer provides accurate estimate of the states, and the estimation error remains within the theoretical error bounds, up to a certain order of magnitude. The residual error in both cases is small, and can be explained by the numerical errors when implementing a non-smooth observer and model and sensor errors (in experiments).

Future work will focus on output-feedback controller design, using the presented observer. The control goal is to suppress slip-stick oscillations in steady-state.

REFERENCES

[1] N. Mihajlović, A. A. Van Veggel, N. Van de Wouw, and H. Nijmeijer, "Analysis of friction-induced limit cycling in an experimental drill-string set-up," *ASME Journal of Dynamic Systems, Measurements and Control*, 2005.

[2] N. Mihajlović, "Torsional and lateral vibrations in flexible rotor systems with friction," Ph.D. dissertation, Eindhoven University of Technology, The Netherlands, 2005.

[3] J. F. Brett, "Genesis of torsional drillstring vibrations," *SPE Drilling Engineering*, vol. 7, no. 3, pp. 168–174, 1992.

[4] R. I. Leine, D. H. van Campen, and W. J. G. Keultjes, "Stick-slip whirl interaction in drillstring dynamics," *ASME Journal of Vibrations and Acoustics*, vol. 124, pp. 209–220, 2002.

[5] E. Kreuzer and O. Kust, "Analyse selbsterregter drehschwingugnen in torsionsstäben," *ZAMM - Journal of Applied Mathematics and Mechanics / Zeitschrift fuer Angewandte Mathematik und Mechanik*, vol. 76, no. 10, pp. 547–557, 1996a.

[6] F. Pfeiffer and M. Hajek, "Slip-stick motions of turbine blade dampers," *Phil. Trans. Roy. Soc. Lond. A*, vol. 338, no. 9, pp. 503–517, 1992.

[7] R. H. A. Hensen, "Controlled mechanical systems with friction," Ph.D. dissertation, Eindhoven University of Technology, The Netherlands, 2002.

[8] E. Cataldi and C. Glocker, "Curve squealing of railroad vehicles," in *Proceedings of the 5th EUROMECH Nonlinear Oscillations Conference*, Eindhoven, The Netherlands, August 1–12 2005, pp. 1970–1976.

[9] A. Juloski, "Observer design and identification methods for hybrid systems: theory and experiments," Ph.D. dissertation, Eindhoven University of Technology, 2004.

[10] W. Heemels, A. Juloski, and B. Brogliato, "Observer design for Lur'e systems with multi-valued mappings," in *Proceedings of the IFAC World Congress*, Prague, Czech Republic, 2005.

[11] J. Aubin and A. Cellina, *Differential Inclusions*. Springer–Verlag, Berlin, 1984.

[12] H. Brezis, *Operateurs Maximaux Monotones*. North-Holland/American Elsevier, Amsterdam, 1973.

[13] R. Tyrell Rockafellar, *Convex Analysis*. Princeton University Press, Princeton, New Jersey, 1970.

[14] J. Wen, "Time domain and frequency domain conditions for strict positive realness," *IEEE Transactions on Automatic Control*, vol. 33, no. 10, pp. 988–992, 1988.

[15] M. Arcak and P. Kokotović, "Observer based control of systems with slope-restricted nonlinearities," *IEEE Transactions on Automatic Control*, vol. 46, no. 7, pp. 1146–1150, 2001.

[16] A. Dontchev and F. Lempio, "Difference methods for differential inclusions," *SIAM review*, vol. 34, no. 2, pp. 263–294, 1992.

[17] A. Kastner-Maresch, "Implicit Runge-Kutta methods for differential inclusions," *Numererical fuctional analysis and applications*, pp. 937–958, 1991.

[18] M. Vidyasagar, *Nonlinear Systems Analysis*. Prentice Hall, Englewood Cliffs, New Jersey, 1993.

[19] A. Filippov, *Differential Equations with Discontinuous Righthand Sides*, ser. Mathematics and its Applications. Dordrecht, The Netherlands: Kluwer, 1988.

[20] R. I. Leine, D. H. van Campen, A. de Kraker, and L. van den Steen, "Stick-slip vibrations induced by alternate friction models," *Nonlinear dynamics*, vol. 16, pp. 41–54, 1998.